Resilient Power Systems Operation with Offshore Wind Farms and Cloud Data Centers

Shengwei Liu, *Student Member*, *IEEE*, Yuanzheng Li, *Member*, *IEEE*, Xuan Liu, *Student Member*, *IEEE*, Tianyang Zhao, *Member*, *IEEE*, and Peng Wang, *Fellow*, *IEEE*

***Abstract*—To enhance the resilience of power systems with offshore wind farms (OWFs), a proactive scheduling scheme is proposed to unlock the flexibility of cloud data centers (CDCs) responding to uncertain spatial and temporal impacts induced by hurricanes. The total life simulation (TLS) is adopted to project the local weather conditions at transmission lines and OWFs, before, during, and after the hurricane. The static power curve of wind turbines (WTs) is used to capture the output of OWFs, and the fragility analysis of transmission-line components is used to formulate the time-varying failure rates of transmission lines. A novel distributionally robust ambiguity set is constructed with a discrete support set, where the impacts of hurricanes are depicted by these supports. To minimize load sheddings and dropping workloads, the spatial and temporal demand response capabilities of CDCs according to task migration and delay tolerance are incorporated into resilient management. The flexibilities of CDC's power consumption are integrated into a two-stage distributionally robust optimization problem with conditional value at risk (CVaR). Based on Lagrange duality, this problem is reformulated into its deterministic counterpart and solved by a novel decomposition method with hybrid cuts, admitting fewer iterations and a faster convergence rate. The effectiveness of the proposed resilient management strategy is verified through case studies conducted on the modified IEEE-RTS 24 system, which includes 4 data centers and 5 offshore wind farms.**

***Index Terms*—Cloud computing data center, decomposition, hurricane, offshore wind farm, resilience enhancement, total life simulation, unit commitment.**

NOMENCLATURE

A. Indexes and Sets

$t \in \mathcal{T}$	Time interval set.
$a \in \mathcal{T}$	Time interval set when workloads are collected.
$e \in \mathcal{T}$	Time interval set when workloads are processed.
$w \in \mathcal{W}$	Offshore wind farm set.
$ij \in \mathcal{E}$	Transmission line set.
$l \in \beth_{ij}$	Tower set of transmission line ij.
$k \in \mathcal{K}_{ij}$	Conductor segment set of transmission line ij.
$\omega \in \Omega$	Scenario set.
$\mathbb{P} \in \mathcal{P}$	Ambiguity set.
$c \in \mathcal{C}$	CDC set.
$s \in \mathcal{C}$	Source DC set where the workloads are collected.
$k \in \mathcal{C}$	Destination DC set where the workloads are processed.
$g \in \mathcal{G}$	Generator set.
$d \in \mathcal{D}$	Demand set.
$sk \in \mathcal{A}$	Linkage path set among CDCs.

B. Constants

a_1, a_2, a_3	Coefficients in the hurricane translation speed model.
b_1, b_2, b_3, b_4, b_5	Coefficients in the hurricane heading direction model.
c_1, c_2, c_3	Coefficients in the hurricane intensity model.
RH	Relative humidity.
e_s	Saturation vapor pressure.
x	Ratio of the minimum sustainable surface value of central pressure to the surface value of the partial pressure of ambient dry air.
d_0, d_1	Decay constants.
d	Decay coefficient.
δ	Coriolis parameter.
Ω_r	Earth rotation rate.
h_z	Gradient wind height.
α_r	Surface roughness.
R	Radius of the rotor blades.
C_p	Power conversion coefficient.
ρ_{air}	Air density.
$V_{\text{cut-in}}$	Cut-in wind speed.
V_{rate}	Rated wind speed.
$V_{\text{cut-out}}$	Cut-out wind speed.
P_{rate}	Rated power output of the wind turbine.
N_w	The number of wind turbines in the wind farm.
τ_{DRO}	Total distance tolerance.
η_u	CPU utilization of servers.
$W_{sk}^{\text{bandwidth}}$	Maximum bandwidth capacity.
τ_{deadline}	Time limitation of response to delay-tolerant task.
τ_{delay}	High latency limit.

Manuscript received March 9, 2022; revised May 12, 2022; accepted June 23, 2022. Date of online publication November 17, 2023; date of current version November 20, 2023. This work was supported by the State Key Laboratory of Alternate Electrical Power System with Renewable Energy Sources under Grant LAPS21002, the State Key Laboratory of Disaster Prevention and Reduction for Power Grid Transmission and Distribution Equipment under Grant SGHNFZ00FBYJJS2100047.

S. W. Liu (https://orcid.org/0000-0002-6382-7342) and X. Liu are with Energy and Electricity Research Center, Jinan University, Zhuhai 519070, China.

Y. Z. Li is with Huazhong University of Science and Technology, Wuhan 430074, China.

T. Y. Zhao (corresponding author, email: matrixeigs@gmail.com) is with North China Electric Power University, Beijing 102206, China.

P. Wang is with School of Electrical and Electronic Engineering, Nanyang Technological University, Singapore 639798, Singapore.

DOI: 10.17775/CSEEJPES.2022.01470

ρ_{m}	Power consumption factor of workload migration.
μ	Processing rate of workload in each server.
η_{UE}	Energy consumption coefficient of servers.
P_P	Peak power consumption of servers.
P_{I}	Idle power consumption of servers.
$\boldsymbol{G}, \boldsymbol{E}, \boldsymbol{M}$	Linear matrix for the first stage, second stage and uncertain variables in the second stage optimization problem.
$\boldsymbol{h}$	Constant vector for the second stage optimization problem.
$\boldsymbol{c}, \boldsymbol{d}$	Coefficient vector for the first and second stage objective function.
c^{VOLL}	Cost coefficient for load shedding.
c^{VOGC}	Cost coefficient for generation curtailment.
c^{VOLW}	Cost coefficient for workload dropping.
c_{sk}^{VOMW}	Cost coefficient for workload migration via linkage path sk.
c^{VODW}	Cost coefficient for delayed-workload penalty.
c_g^{start}, c_g^{shut}	Cost coefficients for start-up and shut-down operations of units.
a_g, b_g	Fuel cost coefficients of units.
$c_{\mathrm{R},g}$, $c_{\mathrm{r},g}^{+}$, $c_{\mathrm{r},g}^{-}$	Cost coefficients for spinning reserve, regulation up and regulation down reserve.
ρ	Risk-averse factor.
β	Confidence level of conditional value-at-risk.
M_c	Number of servers in the data center.

C. Uncertain Variables

ϵ_v, ϵ_θ, ϵ_I	Random residual terms for simulating hurricane translation speed, heading direction and intensity.
ϵ_B, $\epsilon_{lnR^{\mathrm{mw}}}$	Random residual terms for modeling gradient wind speed.
Δp_d^t	Load forecasting error.
$\pi_{ij,t}$, $\pi_{h,t}$, $\pi_{l,t}$	Failure probabilities of transmission lines, towers and conductor segments.
I_{ij}^t	Status of transmission lines, Binary variable, 1 if line ij is on-line, 0 otherwise.
r	Distance between the site and the hurricane eye.
$A_{r,t}$, B_t	Scaling parameters.
$V_{r,t}^{\mathrm{gw}}$	Gradient wind speed.
$V_{r,z,t}$	Wind speed considering height.
V_w^t	Wind speed at the hub height of the wind turbine.
$P_{w,\max}^t$	Maximum power available from the wind turbine.
L_c^t	Workloads arrival rate.
v_t	Translation speed of the hurricane.
ϕ_t	Latitude of the hurricane.
ϕ_r	Site latitude.
λ_t	Longitude of the hurricane.
λ_r	Site longitude.
θ_t	Heading direction of the hurricane.
I_t	Relative intensity of the hurricane.
Δp_t	Central pressure drop.
Δp_{L}	Central pressure drop when the hurricane makes landfall.
v_{L}	Translation speed when the hurricane makes landfall.
R^{mw}	Radius of maximum wind.
$V_{r,t}^{\mathrm{W}}$	Gradient wind speed.
$\boldsymbol{\xi}_p$	Stochastic vector in scenario p.

D. First-stage Decision Variables

α_g^t, β_g^t	Start-up and shut-down commands, binary variables.
P_g^t	Power generation set point.
R_g^t	Spinning reserve.
P_{ij}^t	Power transferred in day-head scheduling.
Θ_i^t	Power angle of the bus in day-head scheduling.
m_c^t	Number of online servers.
$\boldsymbol{x}$	Decision vector for the first stage.

E. Second-stage Decision Variables

$p_{g,t}^t$	Actual power output of the generator.
p_w^t	Power output of the offshore wind turbine.
$p_{\mathrm{wf},w}$	Power output of the offshore wind farm.
θ_i^t	Power angle in real-time scheduling.
p_{ij}^t	Power transferred in real-time scheduling.
$p_{\mathrm{ls},d}^t$	Load shedding.
p_{ij}^t	Generation curtailment.
$w_{\mathrm{lo},c}^t$	Dropped workload.
w_{de}^t	Delayed workload.
$wt_{sk}^{a,e}$	Delay-tolerant task workloads.
ws_{sk}^t	Delay-sensitive task workloads.
wm_{sk}^t	Amount of migrated workloads.
$p_{\mathrm{m},c}^t$	Power consumption of migrating workload.
p_c^t	Total power consumption of the data center.
w_{de}^t	Workloads responded with high latency.
$\boldsymbol{y}$	Decision vector for the second stage.

F. Abbreviation

OWF	Offshore wind farm.
UC	Unit commitment.
DR	Demand response.
CDC	Cloud data center.
DRO	Distributionally robust optimization.
DC	Data center.
WF	Wind farm.
WT	Wind turbine.
SO	System operator.
CSP	Cloud service provider.
TLS	Total life simulation.
MPPT	Maximum power point tracking.
MBD	Modified Benders decomposition.
MILP	Mixed integer linear programming.

I. Introduction

A. Motivation

RENEWABLE energy sources are accelerating the decarbonization transition of power systems [1]. Along with the maturity of onshore wind development, OWFs are gaining more and more attention due to richer wind energy, steadier wind speed, etc [2]–[4]. During Hurricane Season, power

output of OWFs is affected by mature stage of hurricanes before landfall [5], while the onshore wind farms are typically affected by strong wind and rain after making landfall, i.e., dissipation. As a result, the period that power systems can be tortured is extended, and dual impacts of more uncertain renewable generation and probabilistic failures of transmission lines can lead to an unexpected deficit of power supply resulting in major blackouts and momentary losses [6]. To alleviate such adverse consequences, UC plays a decisive role in proactive management by adapting units' up and down statuses to possible operational conditions. Furthermore, amounts of various reserves, e.g., regulation up/down reserves and spinning reserves, can be prepared in advance and implemented to respond to latent contingencies as needed. Event-based correlation of hurricane impacts on power generation and transmission needs to be considered to make a more specific operation strategy. Besides proactively scheduling generators and power networks, potential merits of emerging DR resources, e.g., CDCs, can be further explored. Novel proactive energy management schemes should be proposed for unity of both offshore and onshore resources towards hurricanes, formulating a more resilient coalition.

B. Literature Review

Security-constrained unit commitment has been widely discussed in existing literature as a powerful tool to cope with fluctuation and intermittency of power generation resulting from high wind penetration. To guarantee high utilization of wind power, an indicator to measure performance of wind accommodation is modeled as chance constraints [7], which are integrated with reliability indices into the optimization problem to maintain a reliable power supply [8]. A two-stage stochastic UC is proposed in [9], in which transmission constraints and contingencies are considered when investigating operating cost impacts of involving high wind penetration. In [10], a versatile probability is adopted to achieve a more accurate description of wind power forecast errors by adapting the shape parameters to the training data. Regrading strong spatial correlation among geo-distributed WFs, the Dirichlet process mixture model is employed to construct a data-driven uncertainty set of wind power forecast errors for robust UC in a non-parametric paradigm [11]. Similarly, a multidimensional joint probability based on the Gaussian mixture model is applied in [12] to explore the spatial correlation between WFs and lead to a more straightforward solution method of chance-constrained UC optimization.

There has been extensive research on system reliability regarding unexpected and independent outages of power gird elements, e.g., generators and transmission lines in general. To meet requirement of continuous power supply and delivery under accepted standards [13], $N-1$, $N-1-1$, and $N-k$ criteria are broadly implemented in reliability evaluation. Ensuring the system is $N-1$ compliant, co-optimization of transmission topology switching and UC model is proposed in [14] to fetch an optimal transmission switching scheme for cost reduction. Considering the exponential growth of combinatorial contingency states as k increases, full contingency enumeration is unrealistic, and a contingency selection technique has been developed to identify critical components and construct a reduced set of credible contingencies [15], [16]. Instead of relying on a limited contingency list, a robust UC optimization method is proposed in [17] subject to all combinations of most K unit outages in a computationally efficient manner. In [18], an ambiguity set based on the discrete reference scenario set, which combines the most probable contingencies and highest impact contingencies, is embedded into the DRO model to make a transmission system hardening plan.

Normally, power systems are designed to be reliable in normal conditions, while resilience against low-probability and high-impact disruption, e.g., natural disasters and man-made attacks, remains vulnerable [19], [20]. Existing strategies for resilience enhancement can be generally divided into prevention [21]–[23], emergency response [24]–[27] and restoration [28], [29]. This paper falls under day-ahead preventive actions and real-time emergency response, so only relevant research will be discussed. In [19], power flow entropy and power line loading rate are treated as penalty terms in the objective function of the proposed resilience-constrained UC, in which weather intensity is normalized into normal, severe conditions and major storm disaster, and impacts of certain weather events are not revealed. A resilient operation method is presented for distribution systems in [24], which collaborates deep reinforcement learning as a tool to train an intelligent controller. During the training process, various translation speeds and approaching angles are given to generate straight hurricane traces with constant intensity overseas. In [25], differences between prevailing and event-related uncertainties are discussed. Fragility curves estimate a dynamic uncertainty bound of operation conditions based on historical data for microgrid operators. Resilient operation based on an ambiguity set of branch outages considering uncertainties of probability distribution is proposed in [23], and [27] for transmission and distribution systems, respectively. Weather condition is assumed to be idle at different locations at the same time for distribution systems, while in transmission systems it varies at spatially distributed components.

With spatially DCs, CDCs have been recognized as temporal and spatial flexible DR resources by exploring different characteristics of workloads. For given workloads arrival sequence, temporal flexibility is realized by a single DC, by optimally scheduling delay-tolerant and delay-sensitive workloads, using dynamic voltage frequency scaling [30], [31] and dynamic power management [32]–[34]. Further adjusting arrival sequence of workloads via migrating workloads among different DCs, CDCs can realize power load shifting among DCs spatially. This ability has been deployed to improve operational efficiency of CDCs under normal conditions, e.g., reducing power consumption and monetary cost [35], [36]. Besides energy-saving strategies for cloud service providers, CDCs are recently coordinated into novel application scenarios, e.g., operation cost reduction for power systems [37], flexibility improvement for distribution network [38], generation and transmission expansion postponement [39]. It has not been verified whether spatial flexibility of CDCs can be employed in UC problems during the proactive management during extreme events.

Despite strenuous efforts, some gaps remain to be further explored in resilient operation strategies. Numerous parametric and non-parametric probability distributions have been developed to describe wind power uncertainty in normal weather conditions appropriately. Extremely high wind speed exceeding cut-out wind speed of WTs during hurricanes is out of consideration, which leads to extreme mechanical load on the structure of WTs. To prevent severe damage, WTs need to be shut down, and power injected from WFs can change from maximum to zero, incurring a substantial and unexpected loss of generation in power systems with high wind penetration. In other words, when hurricanes are passing by, wind speed affects reliability of transmission lines and availability of renewable power generation simultaneously. In most existing literature about resilience enhancement, dual impacts of extreme events on renewable generation and transmission lines are exclusively considered ignoring the event-related nature. To make a more specific operation strategy for resilience enhancement, available output of WTs should be derived from time-varying wind speed at hub height according to the hurricane track.

C. Contributions

To fulfill research gaps mentioned before, a proactive operation strategy is proposed in this paper to enhance resilience of power systems against hurricanes. The strategy combining UC and scheduling of CDCs is modeled as a two-stage DRO problem with risk aversion [40]. The main contributions of this paper compared to existing literature are summarized as follows:

1) Combining the TLS method of hurricanes with the fragility curve of transmission line components and power curve of WTs, an event-based ambiguity set is generated, reflecting underlying correlations between renewable energy fluctuation and failures of transmission lines.

2) Effectiveness of CDCs as a kind of resilient DR resource under extreme conditions is explored, taking advantage of temporal flexibility of delay-tolerant workloads and spatial flexibility via task migration among geo-distributed CDCs.

3) Regarding time-consuming iterations of classical Benders decomposition caused by poor performance of optimal cuts, a novelty decomposition algorithm with hybrid cuts is proposed to speed up the convergent process, which effectively balances scale of the master problem and number of iterations.

II. Proactive Resilient Management of Power Systems Towards Hurricanes

This section presents resilience management of power systems with CDCs and OWFs. As shown in Fig. 1, data and power layers are contained in a coupled system and interact via buses to which CDCs connect. In data layer, the CDC platform consists of several DCs and the data transmission networks among DCs. The nearest front-end proxies of CDCs firstly collect the calculation requests submitted from users and subsequently route to local servers or migrated among CDCs via cyber linkage as needed taking delay tolerance of requests into account [41]. A power transmission network

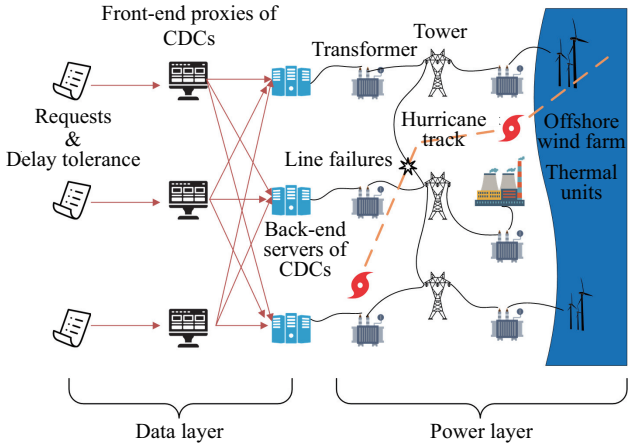

Fig. 1. Power systems with OWFs and CDCs.

integrated with several geographically diverse OWFs is taken into account in the power layer.

According to the uncertainty set obtained by applying TLS illustrated in Section III, a proactive operation strategy is critical for SOs and CSPs. From the perspective of SOs, dual uncertainties from generation and transmission sides pose formidable challenges for maintaining a continuous power supply. In terms of CSPs, loss of power supply can lead to computing task failures and create dissatisfaction towards cloud services [42]. For a more reliable power supply and to avoid workload dropping, CDCs scheduling is integrated with traditional controllable resources, i.e., thermal units, to make a joint two-stage unit commitment, as shown in Fig. 2. Taking advantage of workload migration and the geo-distributed feature of CDCs, power consumption of CDCs could be shifted from one bus to another together with task migration.

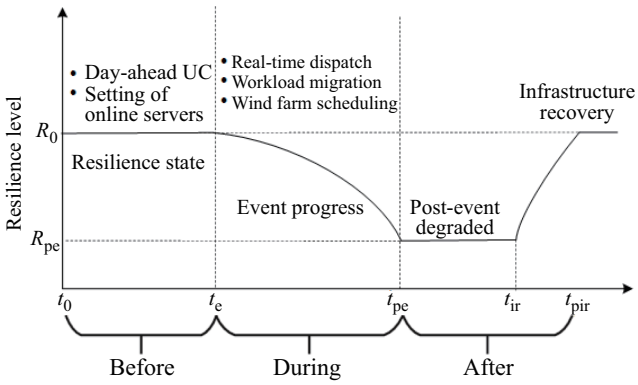

Fig. 2. Framework of the proposed resilient operation strategy.

III. Ambiguity Sets for Operating Scenarios under Hurricanes

Impacts of hurricanes on power systems are explored in this section, including drastic fluctuation of wind power generation caused by critical wind conditions and potential failures of transmission lines due to high wind speed and heavy rain. TLS describes hurricanes' development and dissipation process overseas and onshore in detail. Time-varying intensity and track are combined with wind power curve and fragility curve

to develop an event-based uncertainty set, which is then treated as reference probability distribution of the ambiguity set.

A. Total Life Hurricane Simulation

Several features, e.g., location, intensity, translation speed, heading direction, and the radius of max wind, are essential for simulating a whole life hurricane track with the statistical model [10]. Historical data of hurricanes within the region of interest is utilized to formulate a statistical model. There have been various researches indicating evolution of hurricane trajectory path depends on two time slots before [43], [44]. Time-varying track simulation based on Markov chains is presented as follows:

$$v_t = a_1 + a_2 v_{t-1} + a_3 v_{t-2} + \epsilon_v, \ \forall t \tag{1}$$

$$\theta_t = b_1 + b_2\theta_{t-1} + b_3\theta_{t-2} + b_4\phi_{t-1} + b_5\lambda_{t-1} + \epsilon_\theta, \ \forall t \tag{2}$$

Current hurricane translation speed in time slot t depends on v_{t-1} and v_{t-2}, while current direction is also affected by latitude and longitude one timeslot before.

Intensity simulation model is different onshore and offshore, considering the nature of hurricanes' development and dissipation process. Central pressure drop is widely accepted to depict intensity of hurricanes onshore. Instead, relative intensity is introduced to normalize hurricane intensity overseas, regrading the climatic conditions, e.g., sea surface temperature (SST). Calculation of relative intensity is shown as follows:

$$I_t = \frac{1013 - \Delta p_t + (1 - \mathrm{RH})e_s}{(1-x)[1013 - (\mathrm{RH} \times e_s)]}, \ \forall t \tag{3}$$

$$I_t = c_1 + c_2 I_{t-1} + c_3 I_{t-2} + \epsilon_I, \ \forall t \tag{4}$$

After hurricanes make landfall, the power source which keeps sustaining convection and lowers central pressure of hurricanes is lost. As a result, eye heating gradually decreases, and central pressure increases. The filling model is depicted as follows:

$$\Delta p_t = \Delta p_{\mathrm{L}} \exp(-d\Delta t), \ \forall t \tag{5}$$

$$\Delta t = t - t_{\mathrm{L}}, \ \forall t \tag{6}$$

$$d = d_0 + d_1(\Delta p_{\mathrm{L}} v_{\mathrm{L}} / R^{\mathrm{mw}}) \tag{7}$$

Remark1. According to historical hurricane data, coefficients in the intensity model, translation speed model, heading direction model, i.e., a_1, a_2, a_3 in (1), b_1, b_2, b_3, b_4, b_5 in (2), c_1, c_2, c_1 in (4) are estimated by auto-regressive method with predefined spatial grids and time frames. Randomness of hurricanes mainly relies on residual terms, i.e., ϵ_v, ϵ_θ, ϵ_I, which generally do not follow normal distribution [10]. Empirical distributions are employed to depict these terms. The initial state of location, intensity, and heading direction is known under the assumption it could be obtained from the bureau of meteorology.

To quantify the wind speed at WTs and transmission lines, the wind field model, which reflects physical characteristics of hurricanes, is used [44]. With the distinct distance r from the center of the hurricane, gradient wind speed could be represented as follows:

$$V_{r,t}^{\mathrm{gw}} = [A_{r,t} + \delta^2 r^2/4]^{\frac{1}{2}} - r\delta/2, \ \forall r, t \tag{8}$$

$$A_{r,t} = (R_t^{\mathrm{mw}}/r)^{B_t} B_t \Delta p \frac{\exp(-(R_t^{\mathrm{mw}}/r)^{B_t})}{\rho_{\mathrm{air}}}, \ \forall r, t \tag{9}$$

$$B_t = 1.881 - 0.00557 R_{\mathrm{mw}} - 0.01295\phi_t + \epsilon_B, \ \forall t \tag{10}$$

$$\ln R_t^{\mathrm{mw}} = 3.859 - 7.7001 \times 10^{-5}\Delta p_t^2 + \epsilon_{\ln R^{\mathrm{mw}}}, \ \forall r, t \tag{11}$$

$$\delta_r = 2\Omega_r \sin\phi_r, \ \forall r, t \tag{12}$$

In the vertical direction, increase of wind speed with the height model in [45] is utilized to distinguish wind speed at different heights z. It is shown as follows:

$$V_{r,z,t} = V_{r,t}^{\mathrm{gw}} \left(\frac{h}{h_z}\right)^{\alpha_r}, \ \forall r, z, t \tag{13}$$

Integrating the wind field model with time-varying intensity and track model, a specific hurricane scenario can be generated by hurricane information of the initial time slot, i.e., central pressure drop, translation speed, and heading direction.

B. Power of Offshore Wind Farm Output

The power generated by a WT depends on wind speed at the hub site and power conversion coefficient of the WT. The power output available from a WT $P_{w,\max}^t$ is shown as follows:

$$P_{w,\max}^t = \begin{cases} 0, & V_w^t \in [0, V_{\text{cut-in}}], \\ \frac{1}{2}\rho_{\mathrm{air}}\pi R^2 (V_{\mathrm{w}}^t)^3 C_p, & V_w^t \in (V_{\text{cut-in}}, V_{\text{rate}}], \\ P_{\text{rate}}, & V_w^t \in (V_{\text{rate}}, V_{\text{cut-out}}), \\ 0, & V_w^t \in (V_{\text{cut-out}}, +\infty] \end{cases}, \ \forall w, t \tag{14}$$

When wind speed is lower than cut-in speed $V_{\text{cut-in}}$, power output of WTs is 0. In the second wind speed interval between $V_{\text{cut-in}}$ and V_{rate}, available power increases with wind speed. Widely utilized in WT control, MPPT strategy is realized by adjusting the rotational speed, so the power curve under MPPT is assumed to be the upper bound of power generated by WTs. In the third wind speed interval between V_{rate} and $V_{\text{cut-out}}$, power output available stays to be a constant P_{rate}, i.e., the maximum output. However, if the wind speed exceeds $V_{\text{cut-out}}$, WTs are shut down to protect the turbines from extreme mechanical load.

The power output of a WF is shown as follows:

$$0 \le p_w^t \le P_{w,\max}^t, \ \forall t, w \tag{15}$$

$$p_{\mathrm{wf},w}^t = N_w p_w^t, \ \forall t, w \tag{16}$$

In the proposed strategy, power output of WTs can be dispatched down if needed since adaptive rotor speed of the WT could be achieved by adjusting pitch angle and tip speed ratio [46].

C. Modeling of Transmission Line Failures

According to the TLS, a fragility analysis model is introduced to quantify failure probabilities of transmission line components, i.e., towers and segments. The fragility analysis model is based on the discrete-time Markov process, details of which can refer to (1)–(3) in [23].

Combining transmission segments and towers in series, failure probabilities of transmission lines are shown as follows:

$$\pi_{ij,t} = 1 - \prod_{k \in \mathcal{K}_{ij}} (1 - \pi_{k,t}) \prod_{l \in \beth_{ij}} (1 - \pi_{l,t}), \ \forall ij, t \tag{17}$$

The scenario of line failures is generated by comparing $\pi_{ij,t}$ with random number sampled from uniform distribution within [0, 1] interval.

D. Formulation of Ambiguity Sets

A metric-based ambiguity set is proposed to depict uncertain operation conditions, which contains a family of distributions being close to the reference distribution from the point of given statistic distance, i.e., L_1 distance in this paper [40]. Uncertain variables related to operational strategy include power output of WFs, failures of transmission lines, task arrival rate of CDCs, and load forecasting errors. The ambiguity set is shown as follows:

$$\mathcal{P}=\left\{\mathbb{P}:\sum_{\omega\in\Omega}|\pi_{\omega}^{0}-\pi_{\omega}|\leq\tau_{\text{DRO}}\right\} \tag{18}$$

where π_{ω}^{0} and π_{ω} are discrete probabilities of scenario ω in nominal and true distribution, respectively. τ_{DRO} is L_1 distance tolerance. Motivation and detailed merits of the proposed ambiguity set are explained in Remark 2.

Remark2. DRO is a novel approach to handling uncertainties, eliminating the impractical assumption under stochastic optimization that the exact probability distribution of scenarios is known, and alleviates excessive conservatism of robust optimization [47]. With limited data of scenarios, a less-conservative result can be obtained considering worst realization of probability distribution within the ambiguity set. Compared to existing ambiguity sets in [23], [27], which describe only impacts of hurricanes on branch outage probability, a more comprehensive ambiguity set is proposed to reflect event-based characteristics including available power output of WFs and failures of transmission lines. In each scenario, the time-varying intensity hurricane track is treated as the same input for both power output model of OWFs and failure model of transmission lines. Rather than assuming different types of uncertain variables are independent, the coupling relationship among uncertainties between generation and transmission sides is considered in the proposed ambiguity set.

IV. Cloud Computing Data Center Modeling for Proactive Management

An appropriate number of online servers within each DC should be determined in day-ahead UC, considering high energy consumption of idle servers and delay during the transition between sleep state and active state. Idle servers in CDCs are usually over-provisioned and set as active to meet peak requests. However, power consumed by an idle server is more than 60% of peak power [48]. From the perspective of energy saving, idle servers should be turned off or switched into deep-sleep modes [34]. Considering long setup time spent to turn them back on before they could process workloads, proactive management of online servers is essential to pre-schedule CDCs, which is shown as follows:

$$m_{c}^{t}\leq M_{c},\ \forall c,t \tag{19}$$

Referring to [41], [49], workloads at each DC could be reallocated among CDCs via optical fibers as needed in real-time scheduling of CDCs, according to arrival rate and delay tolerance of requests. Management model of CDCs during real-time scheduling is shown as follows:

$$0\leq wt_{sk}^{a,e},\ \forall sk,a,e \tag{20}$$

$$0\leq ws_{sk}^{t},\ \forall sk,t \tag{21}$$

$$L_{c}^{t}=\sum_{e\in\mathcal{T}}\sum_{k\in\mathcal{C}}wt_{sk}^{a,e}+\sum_{k\in\mathcal{C}}ws_{sk}^{t},\ \forall c,t \tag{22}$$

$$V_{c}^{t}=\sum_{a\in\mathcal{T}}\sum_{s\in\mathcal{C}}wt_{sk}^{a,e}+\sum_{s\in\mathcal{C}}ws_{sk}^{t}-w_{\text{lo},c}^{t},\ \forall c,t \tag{23}$$

$$V_{c}^{t}=m_{c}^{t}\eta_{\text{u},c}^{t}\mu,\ \forall c,t \tag{24}$$

$$0\leq\eta_{\text{u}}\leq 1 \tag{25}$$

$$wt_{sk}^{a,e}=0,\ \forall sk,a-e>\tau_{\text{deadline}} \tag{26}$$

$$wm_{sk}^{t}=\sum_{a\in\mathcal{T}}wt_{sk}^{a,e}+ws_{sk}^{t},\ \forall sk,t \tag{27}$$

$$wm_{sk}^{t}\leq W_{sk}^{\text{bandwidth}},\ \forall sk,t \tag{28}$$

$$p_{\text{m},c}^{t}=\rho_{\text{m}}\left(\sum_{k\in\mathcal{C},k\neq c}wm_{ck}^{t}+\sum_{s\in\mathcal{C},s\neq c}wm_{\text{sc}}^{t}\right),\ \forall t,c \tag{29}$$

$$(P_{\text{I}}+(\eta_{\text{UE}}-1)P_{P})m_{c}^{t}+(P_{P}-P_{\text{I}})\frac{V_{c}^{t}}{\mu}+p_{\text{m},c}=p_{c}^{t},\quad\forall m,c,t \tag{30}$$

$$w_{\text{de}}^{t}=\sum_{a\in\mathcal{T},a-t\geq\tau_{\text{delay}}}\sum_{sk\in\mathcal{A}}wt_{sk}^{a,t},\ \forall t \tag{31}$$

Equations (20)–(24) are constraints on task collection and processing balance. Equation (25) is constraint of CUP utilization under the assumption that all servers in the CDCs are homogeneous and workloads are equally distributed and could be calculated in parallel. Equation (26) represents workloads that must be responded to within the time limitation. Equations (27) and (28) are balances of workload migration and capacity limitation. Equations (29) and (30) denote power consumption of CDCs after workload redistribution. Equation (31) counts sum of tasks responded with high latency, which incurs delay penalty.

While CDCs' temporal and spatial flexibility is exploited to enhance system resilience, cost associated with DR of CDCs should be considered, including extra energy consumption and bandwidth cost for migrating workloads among CDCs in (29) and (34) later in Section V, and penalty due to dissatisfaction towards high-latency response in (31) and (34) [41], [50], [51]. Generally, CSPs are mainly concerned about reliable power supply and energy cost-saving, which is the immanent incentive for CDCs to participate in the DR program is increase of net benefit [37]. However, the specific redistribution mechanism of social welfare by applying resilient operation remains undiscussed here because this paper pays more attention to exploring effectiveness of CDCs as a kind of resource in resilient management.

V. Distributionally Robust Unit Commitment for Resilient Operation

A two-stage DRO problem describes the decision-making process in day-ahead and real-time operational periods. Day-

ahead UC, including pre-scheduling of CDCs, is assigned at the first stage. Real-time scheduling of generators and workload migration of CDCs are determined at the second stage under each scenario, respectively. DRO problem is then reformulated as a MILP problem, solved by a decomposition method with hybrid cuts, including primal cuts and optimal cuts. Primal cuts are derived from worst scenario and can be updated in each iteration to maintain a small scale of the master problem.

A. Objective Functions

Compact expression of the optimization problem is shown as follows:

$$\min_{\boldsymbol{x}\in\boldsymbol{X}} f(\boldsymbol{x}) + \rho \max_{\mathbb{P}\in\mathcal{P}}\{\mathbb{E}[Q_{\text{DRO}}(\boldsymbol{x},\boldsymbol{\xi})] + 1-\rho)C_{\text{VaR},\beta}[Q_{\text{DRO}}(\boldsymbol{x},\boldsymbol{\xi})]\} \tag{32}$$

where $f(\boldsymbol{x})$ is objective function of the first stage. $\boldsymbol{x}$ are first stage decision variables, within feasible set denoted as $\boldsymbol{X}$. $Q_{\text{DRO}}(\boldsymbol{x},\boldsymbol{\xi})$ is recourse problem representing effect of first stage decision variables to the second stage. $\boldsymbol{\xi}$ is a vector consisting of uncertain variables in the second stage. Conditional value-at-risk C_{VaR} is introduced combining factor ρ to reflect risk aversion to extreme conditions at confidence level β.

The objective function of first stage is comprised of start-up, shut-down, fuel, and reserve costs, as follows:

$$\begin{aligned} f(\boldsymbol{x}) &= \boldsymbol{c}^{\mathrm{T}}\boldsymbol{x} \\ &= \sum_{t\in\mathcal{T}}\sum_{g\in\mathcal{G}}\big\{c_g^{\text{start}}\alpha_g^t + c_g^{\text{shut}}\beta_g^t + b_g u_g^t + [a_g P_g^t \\ &\quad + c_{\text{R},g}R_g^t + c_{\text{r},g}^{+}r_g^{+,t} + c_{\text{r},g}^{-}r_g^{-,t}]\Delta t\big\} \end{aligned} \tag{33}$$

The objective function in the second stage, which reveals impacts of the hurricane, is presented as follows:

$$\begin{aligned} Q_{\text{DRO}}(\boldsymbol{x},\boldsymbol{\xi}) &= \min_{\boldsymbol{y}\in\mathcal{Y}(\boldsymbol{x},\boldsymbol{\xi})} \boldsymbol{d}^{\mathrm{T}}\boldsymbol{y}_\omega \\ &= c^{\text{VOLL}}\sum_{t\in\mathcal{T}}\sum_{d\in\mathcal{D}} p_{\text{ls},d}^t\Delta t + c^{\text{VOGC}}\sum_{t\in\mathcal{T}}\sum_{g\in\mathcal{G}} p_{\text{gc},g}^t\Delta t \\ &\quad + c^{\text{VOLW}}\sum_{t\in\mathcal{T}}\sum_{c\in\mathcal{C}} w_{\text{lo},c}^t + \sum_{t\in\mathcal{T}}\sum_{sk\in\mathcal{A}} c_{sk}^{\text{VOMW}} wm_{sk}^t \\ &\quad + c^{\text{VODW}}\sum_{t\in\mathcal{T}} w_{\text{de}}^t \end{aligned} \tag{34}$$

where $\mathcal{Y}$ is the feasible set of $\boldsymbol{y}$. $\mathcal{Y}$ is determined by constraints in the second stage.

B. Constraint Sets

Constraints on day-ahead UC consist of start-up and shut-down constraints considering minimum up/downtime, system requirements of spinning and regulation reserve, and number of online servers in CDCs. Constraints on real-time scheduling include ramp-up/down and maximum/minimum power generation constraints of generators, constraints on power transmission considering line failures, load fluctuation limits, real-time management constraints of CDCs, and power balance at each bus. More details about two-stage UC can be referred to (19)–(36) for the first stage and (37)–(42) for second stage in [23]. Besides, power balance constraints considering CDCs and OWFs are presented as follows:

$$\begin{aligned} &\sum_{g\in\mathcal{G}_j}(p_{g,t} - p_{\text{gc},g}^t) + \sum_{ij} p_{ij}^t - \sum_{ij} p_{ji}^t + \sum_{w\in\mathcal{W}_j} p_{\text{wf},w}^t \\ &= \sum_{d\in\mathcal{D}_j}(P_d^t + \Delta p_d^t - p_{\text{ls},d}^t) + \sum_{c\in\mathcal{C}_j} p_c^t,\ \forall t, j \end{aligned} \tag{35}$$

where $\mathcal{W}_j, \mathcal{C}_j$ denote the set of wind farms and DCs connected to bus j, $d\in\mathcal{D}_j$ is load set of the bus j.

C. Deterministic Reformulation and Solution Methods

The optimization problem in (32) is a min-max problem, which could not be solved directly [40]. The Lagrangian dual is utilized to derive the corresponding deterministic counterpart of (32) as follows:

$$\begin{aligned} &\min \boldsymbol{c}^{\mathrm{T}}\boldsymbol{x} + \tau_{\text{DRO}} z + (1-\rho)\eta + \sum_{\omega\in\Omega}\pi_\omega^0(z_\omega^+ - z_\omega^-) + \vartheta \\ &\text{s.t. } \boldsymbol{G}\boldsymbol{x} + \boldsymbol{W}\boldsymbol{y}_\omega \geq \boldsymbol{h} - \boldsymbol{M}\boldsymbol{\xi}_\omega,\ \forall\omega\in\Omega \\ &\quad \rho\boldsymbol{d}_\omega^{\mathrm{T}}\boldsymbol{y}_\omega + \frac{1-\rho}{1-\beta}v_\omega \leq z_\omega^+ - z_\omega^- + \vartheta,\ \forall\omega\in\Omega \\ &\quad z_\omega^+ + z_\omega^- - z \leq 0,\ \forall\omega\in\Omega \\ &\quad \boldsymbol{d}_\omega^{\mathrm{T}}\boldsymbol{y}_\omega - \eta \leq v_\omega,\ \forall\omega\in\Omega \\ &\quad z, z_\omega^+, z_\omega^-, v_\omega \geq 0,\ \boldsymbol{x}\in\boldsymbol{X} \end{aligned} \tag{36}$$

where z, z_ω^+, z_ω^- and ϑ are Lagrangian multipliers of the dual problem. η is value-at-risk (VaR) of the recourse problem Q_{DRO}. $\boldsymbol{X}$ is determined by constraints in first stage optimization, i.e., proactive management of CDCs and day-ahead UC. $\boldsymbol{G}\boldsymbol{x} + \boldsymbol{W}\boldsymbol{y}_\omega \geq \boldsymbol{h} - \boldsymbol{M}\boldsymbol{\xi}_\omega$ are constrains in the second stage optimization, i.e., real-time management of CDCs and economic dispatch. The first and second stage constraints are described in Section V-B.

Considering the increasing scale of the MILP problem as number of scenarios increases, a kind of modified MBD with hybrid cuts is proposed to accelerate convergence and reduce computation time. First, subproblem of each scenario $Q_{\text{DRO}}(\boldsymbol{x},\boldsymbol{\xi}_{\omega*})$ in (34) can be solved independently with given $\boldsymbol{x}$. The scenario index with max operational cost in the second stage is recorded as $\omega*$. The master problem could be formulated as follows:

$$\begin{aligned} &\min \boldsymbol{c}^{\mathrm{T}}\boldsymbol{x} + \tau_{\text{DRO}} z + (1-\rho)\eta + \sum_{\omega\in\Omega}\pi_\omega^0(z_\omega^+ - z_\omega^-) + \vartheta \\ &\text{s.t. } \boldsymbol{\varpi}_\omega^{n,\boldsymbol{T}}(\boldsymbol{h} - \boldsymbol{G}\boldsymbol{x} - \boldsymbol{M}\boldsymbol{\xi}_\omega) - \eta \leq v_\omega,\ \forall\omega\in\Omega,\ \forall n\leq m \\ &\quad \rho\boldsymbol{\varpi}_\omega^{n,\boldsymbol{T}}(\boldsymbol{h} - \boldsymbol{G}\boldsymbol{x} - \boldsymbol{M}\boldsymbol{\xi}_\omega) + \frac{1-\rho}{1-\beta}v_\omega \leq \\ &\qquad z_\omega^+ - z_\omega^- + \vartheta,\ \forall\omega\in\Omega,\ \forall n\leq m \\ &\quad z_\omega^+ + z_\omega^- - z \leq 0,\ \forall\omega\in\Omega \\ &\quad \boldsymbol{G}\boldsymbol{x} + \boldsymbol{W}\boldsymbol{y}_{\omega*} \geq \boldsymbol{h} - \boldsymbol{M}\boldsymbol{\xi}_{\omega*} \\ &\quad \boldsymbol{d}^{\mathrm{T}}\boldsymbol{y}_{\omega*} - \eta \leq v_{\omega*} \\ &\quad \rho\boldsymbol{d}_\omega^{\mathrm{T}}\boldsymbol{y}_{\omega*} + \frac{1-\rho}{1-\beta}v_{\omega*} \leq z_{\omega*}^+ - z_{\omega*}^- + \vartheta \\ &\quad z, z_\omega^+, z_\omega^- v_\omega \geq 0,\ \boldsymbol{x}\in\boldsymbol{X} \end{aligned} \tag{37}$$

where the first and second constraints in the master problem are optimal cuts of classic Benders Decomposition (BD).

Considering load shedding, workload dropping and generation curtailment, second stage optimization problem is always feasible with given $\boldsymbol{x}$ and $\boldsymbol{\xi}$, i.e., $Q_{\text{DRO}}(\boldsymbol{x},\boldsymbol{\xi})$ is a complete recourse problem. $\boldsymbol{\varpi}_{\omega}^{\text{T}}$ are dual variables of second stage subproblem Q_{DRO}. m is the number of iterations. The third to fifth constraints are primal cuts generated according to the most costly scenario and utilized to accelerate convergence. Index $\omega*$ is updated in each iteration, and primal cuts are replaced simultaneously. The scale of the optimization problem remains relatively small, and number of decision variables is invariable during iterations.

$\boldsymbol{\varpi}_{\omega}^{\text{T}}$ can be determined by solving the dual problem shown as follows:

$$\begin{aligned} & Q'_{\text{DRO}}(\boldsymbol{x},\boldsymbol{\xi}_{\omega}) = \max \boldsymbol{\varpi}_{\omega}^{\text{T}}(\boldsymbol{h}-\boldsymbol{G}\boldsymbol{x}-\boldsymbol{M}\boldsymbol{\xi}_{\omega}) \\ & \text{s.t.} \quad \boldsymbol{E}^{\text{T}}\boldsymbol{\varpi}_{\omega} = \boldsymbol{d}, \boldsymbol{\varpi}_{\omega} \geq 0 \end{aligned} \tag{38}$$

With $\boldsymbol{x}^m$ by solving the master problem during iteration m, Q'_{DRO} can be calculated in (38). Then the upper bound during iteration m can be calculated by solving the problem as follows:

$$\begin{aligned} & \min \boldsymbol{c}^{\text{T}}\boldsymbol{x}^m + \tau_{\text{DRO}} z + (1-\rho)\eta + \sum_{\omega\in\Omega} \pi_{\omega}^{0}(z_{\omega}^{+}-z_{\omega}^{-}) + \vartheta \\ & \text{s.t. } \rho Q'_{\text{DRO}}(\boldsymbol{x}^m,\boldsymbol{\xi}_{\omega}) + \frac{1-\rho}{1-\beta} v_{\omega} \leq z_{\omega}^{+} - z_{\omega}^{-} + \vartheta, \ \forall \omega \in \Omega \\ & \quad z_{\omega}^{+} + z_{\omega}^{-} - z \leq 0, \ \forall \omega \in \Omega \\ & \quad Q'_{\text{DRO}}(\boldsymbol{x}^m,\boldsymbol{\xi}_{\omega}) - \eta \leq v_{\omega}, \ \forall \omega \in \Omega \\ & \quad z, z_{\omega}^{+}, z_{\omega}^{-}, v_{\omega} \geq 0 \end{aligned} \tag{39}$$

The complete pseudocode of the MBD is demonstrated as Algorithm 1.

Theorem1. Algorithm 1 converges in fewer iterations than classic Benders Decomposition.

Proof: See appendix for details.

Algorithm 1: Modified Benders Decomposition with optimal and primal cuts

Data: $\boldsymbol{X}, \boldsymbol{G}, \boldsymbol{W}, \boldsymbol{h}, \boldsymbol{M}, \boldsymbol{\xi}_{\omega}, m_{\max}, \varepsilon, \rho, \boldsymbol{c}, \boldsymbol{d}$
Result: $\boldsymbol{x}$, $\boldsymbol{u}$
Initialize: $UB \leftarrow +\infty, LB \leftarrow -\infty, m \leftarrow 1$
while $((UB-LB)/|UB| > \varepsilon) \wedge (m \geq m_{\max})$ **do**
  Solve master problem in (37)
  if *infeasible* **then**
    terminate: The optimization problem is infeasible
  else
    $\boldsymbol{x} \leftarrow \boldsymbol{x}^m, LB^* \leftarrow$ Optimal value of (37)
    $LB \leftarrow \max(LB^*, LB)$.
  end
  for $\omega \in \Omega$ **do**
    Solve the subproblem in (38),
    $\boldsymbol{\varpi}_{\omega}^{n,\text{T}} \leftarrow \boldsymbol{\varpi}_{\omega}^{m,\text{T}}$, get$Q'_{\text{DRO}}(\boldsymbol{x}^m,\boldsymbol{\xi}_{\omega})$
  end
  Derive the scenario $\omega*$, according to $Q'_{\text{DRO}}(\boldsymbol{x}^m,\boldsymbol{\xi}_{\omega*}) = \max_{\omega\in\Omega} Q'_{\text{DRO}}(\boldsymbol{x}^m,\boldsymbol{\xi}_{\omega})$.
  Solve the problem in (39),
  $UB^* \leftarrow$ Optimal value of (39)
  $UB \leftarrow \min(UB^*, UB)$.
  Add the Benders optimal cuts, replace the variables $\boldsymbol{y}_{\omega*}$ and the primal cuts according to $\boldsymbol{\varpi}_{\omega}^{n,\text{T}}$ and $\omega*$.
  $m = m+1$.
end

VI. Case Studies

The experimental setup is first introduced, including simulated system and critical parameters of OWFs and CDCs. Several comparative cases based on different operational strategies are designed to verify performance of the proposed strategy to mitigate damage of hurricanes. Finally, calculation efficiency of the proposed MBD method with hybrid cuts is tested in comparison with classic BD approach.

A. Case Description

As shown in Fig. 3, cases are simulated on a modified IEEE-RTS system [52], which contains 4 geographically dispersed CDCs and 5 OWFs. The entire power system onshore is projected to a $150 * 200$ km area [53]. The attached bus and number of servers in each DC are shown in Table I, and parameters of the server refer to [34]. The processing rate of each server is set to 500 tasks per second. The arrival rate of the task is based on request curves in the ForHLR system derived from [54], and hurricane data set, HURDAT2, from [55] is employed to obtain coefficients of hurricanes in the TLS. As shown in Table II, several linkage paths are accessed to constitute the CDC platform. Test cases are accomplished on a server with an Intel Xeon Gold 6226R CPU@2.90 GHz and 128 GB of RAM. The proposed optimization model is solved by GUROBI.

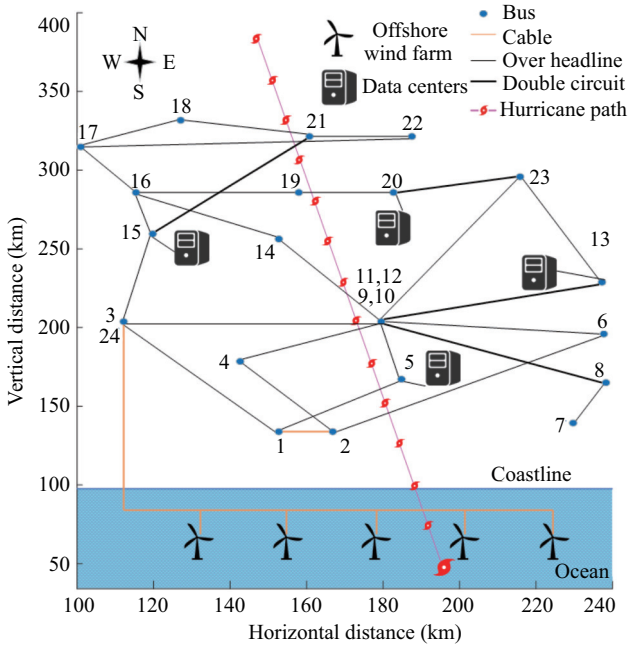

Fig. 3. Modified IEEE-RTS system with CDCs and OWFs.

A total of 5 wind farms are integrated into the power system, located along the coast and 23 km from the coast.

TABLE I
PARAMETERS OF CDCS AND SERVERS

DC	Bus	Quantity of servers	P_P (W)	P_I (W)	η_{UE}
1	5	28000	243	150	1.4
2	13	35000	243	150	1.4
3	15	28000	243	150	1.4
4	20	35000	243	150	1.4

TABLE II
LINKAGE PATHS AMONG CDCS

Path	1	2	3	4	5	6
Source DC	1	1	2	3	4	4
Destination DC	2	3	4	4	1	2
Distance (km)	80.89	112.74	77.52	117.63	67.48	77.52

The total installed capacity of wind power is 234 MW, and wind power generation is injected into the power system by bus 3. The parameters of WTs are shown in Table III [56]. 50 scenarios are generated considering the total life simulation of the hurricane as described in Section II. There are 2 scenarios, scenarios 29 and 41, where load shedding occurs. Scenario 41 is worst scenario with the most significant number of line failures, i.e., 12 lines failed in this scenario, as shown in Fig. 4. Since differences in position, relative location of WFs and hurricane track produce variant wind speed curves in scenario 41 as shown in Fig. 5. The wind speed at WF 1 and WF 2 is M-shape because the eye of the hurricane passed by the location of these WFs. According to wind field features depicted by (8)–(12), wind is very light in the eye and strongest on the eyewall. During 11:00–13:00, significant reduction of the wind speed at WF 2 is caused by close distance between WF 2 and hurricane eye. Considering wind speed at WFs and power curve under MPPT in (14), available outputs of 5 WFs are shown in Fig. 6. The wind speed at WF 5 from 19:00 to 24:00 and WF 1, 2, 3, and 4 from 20:00 to 24:00 is lower

TABLE III
PARAMETERS OF WIND TURBINES

Type	Capacity (MW)	$V_{\text{cut-in}}$ (m/s)	V_{rate} (m/s)	$V_{\text{cut-out}}$ (m/s)	h_0 (m)
E-82	3	3.0	16.0	34.0	78

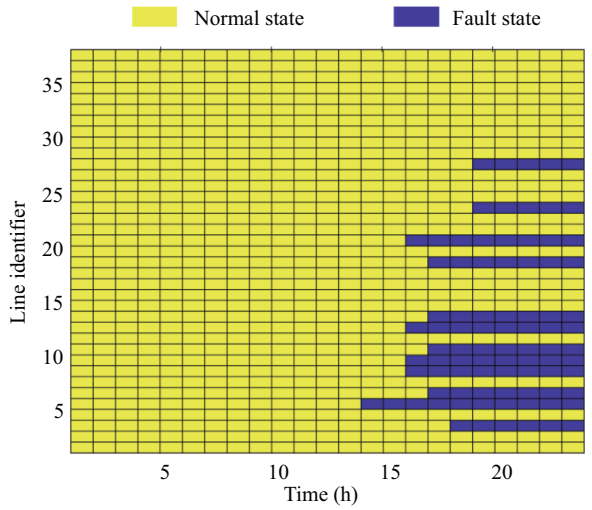

Fig. 4. Line failures in scenario 41.

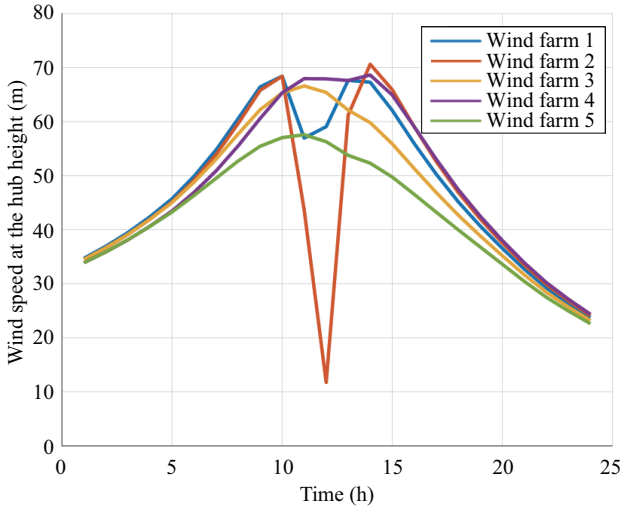

Fig. 5. Wind speed at the hub height in scenario 41.

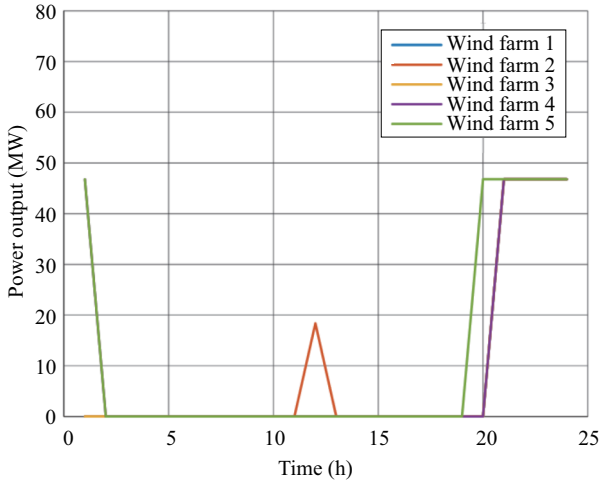

Fig. 6. Power output of OWFs in scenario 41.

than cut-out wind speed and higher than rated wind speed, so maximum wind power outputs are available.

Comparative experiments are first simulated to study impacts of workload flexibility on power balancing. In case 1, workloads are processed by servers in the source DC, by which workload is first collected, and all workloads are set to be delay-sensitive. In case 2, workload migration through the linkage path is considered, and the maximum bandwidth capacity is set to be 2.5×10^6 requests/s, accounting for 25% of peak workload requests. In case 3, both workload migration and workload shifting among different time slots are considered. In case 4, energy-saving scheduling is neglected. Servers in DCs are always active to meet the peak demand of workload requests. To investigate influence of wind power generation, WTs are set to be shut down during operational time in case 5. Maximum service delay of delay-tolerant workloads is set to be 2 hours. ρ_{sen} is ratio of delay-sensitive workloads to all workloads. Moreover, risk-averse impact of the CVaR term in the objective function is explored by setting $\rho = 1$ in case 6 and $\rho = 0$ in case 7. Sustain comparability, all cases are calculated by setting τ_{DRO} and β to be 0.05

and 0.9 correspondingly. $\rho_{\text{bandwidth}}$ is the ratio of maximum bandwidth capacity to peak workload requests. I_{e} and I_{w} are binary variables. $I_{\text{e}} = 1$ means the strategy considers energy-saving, 0 otherwise. $I_{\text{w}} = 1$ means the available wind power is considered, 0 otherwise. These comparative simulated cases are shown in Table IV.

B. Impact of CDCs' Flexibility

Optimization results of different strategies are presented as Table V. κ is optimal value of $C_{\text{VaR},\beta}\left[Q_{\text{DRO}}(\boldsymbol{x},\boldsymbol{\xi})\right]$ in (32). Simulated scenarios have not caused dropped workload and generation curtailment. The cost of workload migration and delay penalty is much less than dropped workload, so the cost in the second stage is mainly caused by load shedding on the demand side. In all cases, $\mathbb{E}[Q_{\text{DRO}}]$ is much smaller than κ, which reflects the extreme operational cost with conditional value β of 0.9. $C_{\text{VaR},\beta}[\sum w_{\text{mi}}]$ is 0 in case 1, because spatial migration and temporal shifting of workload is not allowed. The workload has to be processed locally in time to avoid dropping workload. The number of active servers in each DC is shown in Fig. 7. As shown in Fig. 7, online servers in each DC during operational time are almost the same in case 1 to satisfy requests. However, taking advantage of temporal and spatial flexibility of workloads, the number of active servers in case 3 is optimized to reduce the cost of load shedding. Compared to case 1, load shedding is reduced via task migration in CDCs.

To further research the effect of strategy in extreme conditions, scenarios 29 and 41 are investigated. In scenario 29, transmission lines 3 and 9 failed at 15:00 and 16:00, respectively. As a result, power supply of bus 5 is affected, and load shedding continues until the end of the operational period. Since DC 1 is connected to bus 5, power consumption of active servers in DC 1 could aggravate load shedding in bus 5. In case 2 and case 3, workloads could be migrated from source DCs to destination DCs among CDC platforms via linkage paths, as shown in Table II. Therefore, the number of required servers in source DCs and destination DCs are adjustable by considering workload migration. Power consumption for serving workloads can be transferred from buses where source DCs connected to buses with destination DCs connected. In the proposed strategy, flexible power consumption of CDCs is transferred to reduce load shedding. As shown in Fig. 5, all servers in DC 1 are set to be sleep-down from 18:00 to 24:00, because arrived workloads collected by the DC 1 are migrated to DC 2 and DC 3 in case 3. And the power consumption of CDCs are transferred from bus 3 to buses 12 and 13 at the same time.

To exploit the effect of temporal and spatial flexibility of CDCs in resilience enhancement, reduction of load shedding in case 2 and case 3 compared to case 1 is shown in Fig. 8. In case 3, reduction of load shedding is almost the same in case 2 during 18:00–24:00 because the bandwidth of the linkage paths is sufficient to migrate collected workloads, and all delay-sensitive workloads are reallocated to DC 2 and 3. Taking advantage of spatial flexibility, load shedding is reduced in cases 2 and 3. However, load shedding reduction in case 3 is increased by 5.2% compared to case 2, because arrival rates of workloads in DC 1 are 9.9 $\times 10^6$ requests per second, which exceed the total capacity of paths 1 and 2, 5 $\times 10^6$ requests per second. To process the remaining part of workloads, a certain number of servers have to stay active

TABLE IV
SIMULATED CASES

Case	ρ_{sen}	$\rho_{\text{bandwidth}}$	I_{e}	I_{w}	ρ
1	1	0	1	1	0.5
2	1	0.25	1	1	0.5
3	0	0.25	1	1	0.5
4	0	0.25	0	1	0.5
5	0	0.25	1	0	0.5
6	0	0.25	1	1	1
7	0	0.25	1	1	0

TABLE V
OPTIMIZED RESULTS

Case	$f(\boldsymbol{x})$ (10^5\$)	$\mathbb{E}[Q_{\text{DRO}}]$ (10^4\$)	κ (10^5\$)	$C_{\text{VaR}}[\sum p_{\text{ls}}]$ (p.u.)	$C_{\text{VaR}}[\sum w_{\text{mi}}]$ (p.u.)
1	7.77	0.96	9.56	2.39	0
2	7.76	1.01	9.46	2.37	6.99
3	7.82	0.91	9.45	2.36	14.38
4	8.00	0.93	9.74	2.43	16.44
5	7.81	1.07	11.79	2.94	16.06
6	7.64	1.67	9.87	2.46	15.72
7	7.78	0.89	9.44	2.36	17.73

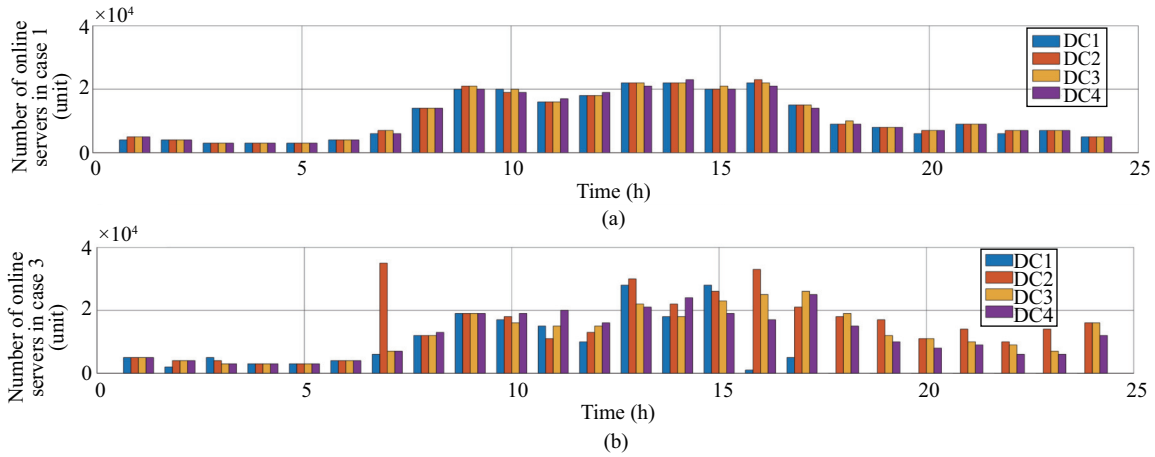

Fig. 7. Number of active servers in CDCs. (a) Case 1. (b) Case 3.

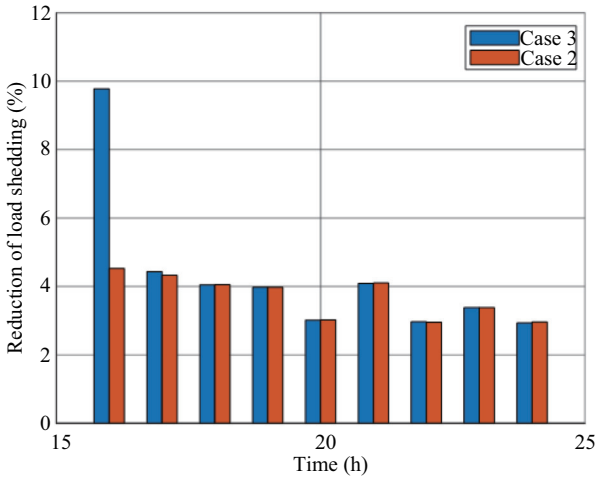

Fig. 8. Reduction of load shedding in scenarios 29 compared to case 1.

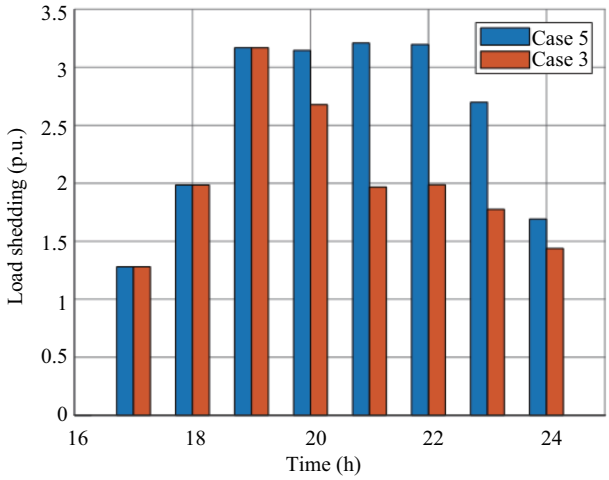

Fig. 9. Comparison of load shedding in scenario 41.

in case 2, leading to extra load shedding compared to case 3. In other words, with consideration of delay tolerance, the performance of CDCs scheduling could be improved since influences of physical constraints, such as the bandwidth capacity constraints and computation capacity constraints, are alleviated or eliminated.

C. Impact of TLS Application

To investigate the effect of application of TLS, all WTs are shut down during the operational time in case 5, while different available power of 5 WFs in case 3 is fetched to make a more resilient operational strategy considering time-varying wind speed and disperse locations as shown in Fig. 6. The optimized results of p_w^{wf} demonstrate power output of WTs in OWFs stays at P_{rate}, which is integrated and injected into bus 3. Severe failures in the transmission network, as shown in Fig. 3, lead to heavy load shedding at several buses, including buses 1, 3, 5, and 6. In case 3, the total load shedding under scenario 41 is 1627 MWh which is 2.8 times load shedding under scenario 29, 591 MWh. Comparison of load shedding in cases 3 and 5 under scenario 41 is shown in Fig. 9. Load shedding during 16:00–19:00 and 23:00–24:00 is mainly due to failures of lines 3, 5, 9, 10, which lead to isolation of buses 5 and 6. Besides, failure of line 6 at 19:00 and line 23 at 20:00 affects power supply at bus 1 and 3, so load shedding occurs is incurred at bus 1 and 3 in case 5. Instead, power shortage at buses 1 and 3 is supplied by timely power injection from wind farms in case 3. Consequently, the total load shedding in case 3 is reduced by 20.1% compared to case 5.

D. Impact of Risk Aversion

Cases 6 and 7 is carried out to investigate effectiveness of risk-averse term $C_{\text{VaR},\beta}[Q_{\text{DRO}}(\boldsymbol{x},\boldsymbol{\xi})]$. In case 6, ρ is set to be 1, which means the operational cost in extreme scenarios is ignored, and proactive management focuses on minimizing the expected value of all scenarios resulting in minimum value of $\mathbb{E}[Q_{\text{DRO}}]$. In contrast, ρ is set to be 0 in case 7, which means the operator is extraordinarily risk-averse and tends to minimize operational cost κ in extreme scenarios. κ in case 7 is reduced by 4.3 $\times 10^4$ compared to case 6, while $f(\boldsymbol{x})$ and $\mathbb{E}[Q_{\text{DRO}}]$ is increased by 1.4 $\times 10^4$ and 7.8 $\times 10^3$, respectively. Extra cost in day-ahead scheduling is incurred to further prevent potentially high penalty in real-time scheduling.

E. Efficiency Analysis of MBD Algorithm

To explore efficiency of the proposed MBD algorithm, the classic BD and the proposed MBD with hybrid cuts are implemented to solve optimization problem (34) with different convergence gaps ϵ and sizes of the scenario set Ns. ρ and β are set to be 0.5 and 0.95, respectively. The number of iterations and computation time Tc are adopted as performance indexes. Convergence performances of BD and MBD are shown in Table VI. Compared with classic BD, BMD significantly reduces both the required number of iterations and computation time. When $Ns = 500$ and $\epsilon = 0.01$, the number of iteration and computation time is reduced by 60.0% and 67.9%, respectively. It reflects the effectiveness of the MBD in coping with a large-scale problem.

TABLE VI
CONVERGENCE RATE COMPARISON

ϵ	Ns	Iteration		Tc (s)	
		BD	MBD	BD	MBD
0.05	10	97	14	158.3	31.3
0.01	10	312	36	961.5	71.8
0.05	100	75	8	630.7	43.37
0.01	100	206	45	10744.1	350.6
0.05	500	43	14	2656.5	531.3
0.01	500	100	40	14665.4	4699.0

In each iteration, $\boldsymbol{\varpi}_\omega$ is determined to generate optimal cuts in (38) with $\boldsymbol{x}^m$, which is obtained by solving the MILP master problem in (37). To guarantee the convergence of the proposed MBD algorithm, only traditional linear programming relaxation and cutting plane method are employed in GUROBI to fetch the exact solution of $\boldsymbol{x}^m$, including Gomory mixed-integer cuts [57], mixed-integer rounding cuts [58] and flow cover cuts [59].

VII. CONCLUSION

Based on the ambiguity set reflecting event-related uncertainties, a proactive operation strategy is proposed for SOs

to enhance system resilience under hurricanes. Several cases are tested at IEEE-RTS systems to validate the effectiveness of the proactive strategy. Considering the temporal and spatial correlation characteristic of hurricane impacts, migration among CDCs and delay tolerance of workload are employed to cope with extreme conditions. As demonstrated in simulation results, CDCs could be treated as a kind of efficient resilient resource to mitigate catastrophic damage of hurricanes. Besides, the proposed MBD algorithm with hybrid cuts can effectively accelerate convergence by reducing the number of iterations and computation time compared to the classic BD method.

APPENDIX
PROOF OF THEOREM 1

Proof: With the constraints $\{\boldsymbol{E}^{\mathrm{T}}\boldsymbol{\varpi}_\omega = \boldsymbol{d}, \boldsymbol{\varpi}_\omega \geq 0\}$ in (38), feasible region of dual variables $\boldsymbol{\varpi}_\omega$ in $Q_{\mathrm{DRO}}{}'(\boldsymbol{x}, \boldsymbol{\xi}_\omega)$ could be denoted by a polyhedron $\mathcal{L}$, and finite set of extreme points in $\mathcal{L}$ is represented by $\mathrm{EP}(\mathcal{L})$. The second-stage optimization problem Q_{DRO} is formulated as a complete recourse problem, $\mathrm{EP}(\mathcal{L}) \neq \emptyset$, and it is assumed there are Q points in $\mathrm{EP}(\mathcal{L})$. According to the Partitioning Theorem in [60], the original problem in (36) is equivalent to the problem as follows:

$$\begin{aligned}
&\min \boldsymbol{c}^{\mathrm{T}}\boldsymbol{x} + \tau_{\mathrm{DRO}} z + (1-\rho)\eta + \sum_{\omega\in\Omega} \pi_\omega^0 (z_\omega^+ - z_\omega^-) + \vartheta \\
&\text{s.t. } \boldsymbol{\varpi}_{q,\omega}^{\mathrm{T}}(\boldsymbol{h}_\omega - \boldsymbol{G}\boldsymbol{x}) - \eta \leq v_\omega,\ \forall\omega\in\Omega,\ \forall q \in \mathrm{EP}(\mathcal{L}) \\
&\quad \rho\boldsymbol{\varpi}_{q,\omega}^{\mathrm{T}}(\boldsymbol{h}_\omega - \boldsymbol{G}\boldsymbol{x}) + \frac{1-\rho}{1-\beta} v_\omega \leq \\
&\qquad z_\omega^+ - z_\omega^- + \vartheta,\ \forall\omega\in\Omega,\ \forall q \in \mathrm{EP}(\mathcal{L}) \\
&\quad z_\omega^+ + z_\omega^- - z \leq 0,\ \forall\omega\in\Omega
\end{aligned} \tag{40}$$

In the proposed algorithm with hybrid cuts, the convergence is guaranteed by the optimal cuts as follows:

$$\begin{aligned}
&\boldsymbol{\varpi}_\omega^{n,\mathrm{T}}(\boldsymbol{h} - \boldsymbol{G}\boldsymbol{x} - \mathrm{M}\boldsymbol{\xi}_\omega) - \eta \leq v_\omega,\ \forall\omega\in\Omega,\ \forall n \leq m \\
&\rho\boldsymbol{\varpi}_\omega^{n,\mathrm{T}}(\boldsymbol{h} - \boldsymbol{G}\boldsymbol{x} - \mathrm{M}\boldsymbol{\xi}_\omega) + \frac{1-\rho}{1-\beta} v_\omega \leq \\
&\quad z_\omega^+ - z_\omega^- + \vartheta,\ \forall\omega\in\Omega,\ \forall n \leq m
\end{aligned} \tag{41}$$

where $\boldsymbol{\varpi}_\omega^{n,\mathrm{T}}$ are derived by solving the subproblem in (38) and added to the master problem during each iteration, and the algorithm that can be terminated before all extreme points are included, i.e., $m \leq Q$.

$\mathrm{G}\boldsymbol{x} + \mathrm{W}\boldsymbol{y}_{\omega*} \geq \boldsymbol{h}_{\omega*}$ are the second stage constraints of scenario $\omega*$, which is most costly during current iteration. All extreme points $\boldsymbol{\varpi}_{q,\omega*}^{\mathrm{T}},\ \forall q \in \mathrm{EP}(\mathcal{W})$ of the worst scenario $\omega*$ are added to master problem by primal cuts as follows:

$$\begin{aligned}
&\mathrm{G}\boldsymbol{x} + \mathrm{W}\boldsymbol{y}_{\omega*} \geq \boldsymbol{h} - \mathrm{M}\boldsymbol{\xi}_{\omega*} \\
&\boldsymbol{d}^{\mathrm{T}}\,\boldsymbol{y}_{\omega*} - \eta \leq v_{\omega*} \\
&\rho\boldsymbol{d}_\omega^{\mathrm{T}}\,\boldsymbol{y}_{\omega*} + \frac{1-\rho}{1-\beta} v_{\omega*} \leq z_{\omega*}^+ - z_{\omega*}^- + \vartheta \\
&z, z_\omega^+, z_\omega^- v_\omega \geq 0,\ \boldsymbol{x} \in \boldsymbol{X}
\end{aligned} \tag{42}$$

In the mth iteration, the number of extreme points considered by optimal cuts is m and the number of extreme points provided by primal cuts is $Q - m$. The extra extreme points effectively improve the lower bound compared to classic Benders Decomposition and result in a fewer number of iterations. It finishes the proof.

REFERENCES

[1] V. M. Nik, A. T. D. Perera, and D. L. Chen, "Towards climate resilient urban energy systems: a review," *National Science Review*, vol. 8, no. 3, pp. nwaa134, Mar. 2021.

[2] R. Perveen, N. Kishor, and S. R. Mohanty, "Off-shore wind farm development: present status and challenges," *Renewable and Sustainable Energy Reviews*, vol. 29, pp. 780–792, Jan. 2014.

[3] Z. Q. Li, S. J. Chen, H. Ma, and T. Feng, "Design defect of wind turbine operating in typhoon activity zone," *Engineering Failure Analysis*, vol. 27, pp. 165–172, Jan. 2013.

[4] E. P. P. Soares-Ramos, L. de Oliveira-Assis, R. Sarrias-Mena, and L. M. Fernández-Ramírez, "Current status and future trends of offshore wind power in europe," *Energy*, vol. 202, pp. 117787, Jul. 2020.

[5] E. B. Watson and A. H. Etemadi, "Modeling electrical grid resilience under hurricane wind conditions with increased solar and wind power generation," *IEEE Transactions on Power Systems*, vol. 35, no. 2, pp. 929–937, Mar. 2020.

[6] National Hurricane Center, "Costliest us U.S. tropical cyclones tables updated," NOAA, Miami, Jan. 2018.

[7] Q. F. Wang, Y. P. Guan, and J. H. Wang, "A chance-constrained two-stage stochastic program for unit commitment with uncertain wind power output," *IEEE Transactions on Power Systems*, vol. 27, no. 1, pp. 206–215, Feb. 2012.

[8] Z. Wu, P. L. Zeng, X. P. Zhang, and Q. Y. Zhou, "A solution to the chance-constrained two-stage stochastic program for unit commitment with wind energy integration," *IEEE Transactions on Power Systems*, vol. 31, no. 6, pp. 4185–4196, Nov. 2016.

[9] A. Papavasiliou and S. S. Oren, "Multiarea stochastic unit commitment for high wind penetration in a transmission constrained network," *Operations Research*, vol. 61, no. 3, pp. 578–592, May 2013.

[10] S. Y. Zhang and K. Nishijima, "Statistics-based investigation on typhoon transition modeling," in *Proceedings of the Seventh International Colloquium on Bluff Body Aerodynamics and Application*, 2012, pp. 364–373.

[11] C. Ning and F. Q. You, "Data-driven adaptive robust unit commitment under wind power uncertainty: a bayesian nonparametric approach," *IEEE Transactions on Power Systems*, vol. 34, no. 3, pp. 2409–2418, May 2019.

[12] Y. Yang, W. C. Wu, B. Wang, and M. J. Li, "Analytical reformulation for stochastic unit commitment considering wind power uncertainty with gaussian mixture model," *IEEE Transactions on Power Systems*, vol. 35, no. 4, pp. 2769–2782, Jul. 2020.

[13] M. Shahidehpour, F. Tinney, and Y. Fu, "Impact of security on power systems operation," *Proceedings of the IEEE*, vol. 93, no. 11, pp. 2013–2025, Nov. 2005.

[14] K. W. Hedman, M. C. Ferris, R. P. O'Neill, E. B. Fisher, and S. S. Oren, "Co-optimization of generation unit commitment and transmission switching with $N-1$ reliability," *IEEE Transactions on Power Systems*, vol. 25, no. 2, pp. 1052–1063, May 2010.

[15] Y. W. Jia, Z. Xu, L. L. Lai, and K. P. Wong, "Risk-based power system security analysis considering cascading outages," *IEEE Transactions on Industrial Informatics*, vol. 12, no. 2, pp. 872–882, Apr. 2016.

[16] P. Kaplunovich and K. Turitsyn, "Fast and reliable screening of N-2 contingencies," *IEEE Transactions on Power Systems*, vol. 31, no. 6, pp. 4243–4252, Nov. 2016.

[17] A. Street, F. Oliveira, and J. M. Arroyo, "Contingency-constrained unit commitment with $n-K$ security criterion: a robust optimization approach," *IEEE Transactions on Power Systems*, vol. 26, no. 3, pp. 1581–1590, Aug. 2011.

[18] A. Bagheri and C. Y. Zhao, "Distributionally robust reliability assessment for transmission system hardening plan under $N-k$ security criterion," *IEEE Transactions on Reliability*, vol. 68, no. 2, pp. 653–662, Jun. 2019.

[19] Y. F. Wang, L. P. Huang, M. Shahidehpour, L. L. Lai, H. L. Yuan, and F. Y. Xu, "Resilience-constrained hourly unit commitment in electricity grids," *IEEE Transactions on Power Systems*, vol. 33, no. 5, pp. 5604–5614, Sep. 2018.

[20] Z. Y. Li, M. Shahidehpour, F. Aminifar, A. Alabdulwahab, and Y. Al-Turki, "Networked microgrids for enhancing the power system resilience," *Proceedings of the IEEE*, vol. 105, no. 7, pp. 1289–1310, Jul. 2017.

[21] S. S. Ma, B. K. Chen, and Z. Y. Wang, "Resilience enhancement strategy for distribution systems under extreme weather events," *IEEE Transactions on Smart Grid*, vol. 9, no. 2, pp. 1442–1451, Mar. 2018.

[22] M. Panteli, D. N. Trakas, P. Mancarella, and N. D. Hatziargyriou, "Power systems resilience assessment: hardening and smart operational enhancement strategies," *Proceedings of the IEEE*, vol. 105, no. 7, pp. 1202–1213, Jul. 2017.

[23] T. Y. Zhao, H. J. Zhang, X. C. Liu, S. H. Yao, and P. Wang, "Resilient unit commitment for day-ahead market considering probabilistic impacts of hurricanes," *IEEE Transactions on Power Systems*, vol. 36, no. 2, pp. 1082–1094, Mar. 2021.

[24] M. M. Hosseini and M. Parvania, "Resilient operation of distribution grids using deep reinforcement learning," *IEEE Transactions on Industrial Informatics*, vol. 18, no. 3, pp. 2100–2109, Mar. 2022.

[25] A. Hussain, A. O. Rousis, I. Konstantelos, G. Strbac, J. Jeon, and H. M. Kim, "Impact of uncertainties on resilient operation of microgrids: a data-driven approach," *IEEE Access*, vol. 7, pp. 14924–14937, Jan. 2019.

[26] T. Ding, M. Qu, Z. K. Wang, B. Chen, C. Chen, and M. Shahidehpour, "Power system resilience enhancement in typhoons using a three-stage day-ahead unit commitment," *IEEE Transactions on Smart Grid*, vol. 12, no. 3, pp. 2153–2164, May 2021.

[27] Y. Z. Zhou, Z. N. Wei, M. Shahidehpour, and S. Chen, "Distributionally robust resilient operation of integrated energy systems using moment and wasserstein metric for contingencies," *IEEE Transactions on Power Systems*, vol. 36, no. 4, pp. 3574–3584, Jul. 2021.

[28] G. Huang, J. H. Wang, C. Chen, J. J. Qi, and C. X. Guo, "Integration of preventive and emergency responses for power grid resilience enhancement," *IEEE Transactions on Power Systems*, vol. 32, no. 6, pp. 4451–4463, Nov. 2017.

[29] Y. P. Fang and G. Sansavini, "Optimum post-disruption restoration under uncertainty for enhancing critical infrastructure resilience," *Reliability Engineering & System Safety*, vol. 185, pp. 1–11, May 2019.

[30] A. Gandhi, M. Harchol-Balter, R. Das, and C. Lefurgy, "Optimal power allocation in server farms," *ACM SIGMETRICS Performance Evaluation Review*, vol. 37, no. 1, pp. 157–168, Jun. 2009.

[31] M. E. T. Gerards, J. L. Hurink, and J. Kuper, "On the interplay between global DVFS and scheduling tasks with precedence constraints," *IEEE Transactions on Computers*, vol. 64, no. 6, pp. 1742–1754, Jun. 2015.

[32] D. Niyato, S. Chaisiri, and L. B. Sung, "Optimal power management for server farm to support green computing," in *Proceedings of the 9th IEEE/ACM International Symposium on Cluster Computing and the Grid*, 2009, pp. 84–91.

[33] F. M. Liu, Z. Zhou, H. Jin, B. Li, B. C. Li, and H. B. Jiang, "On arbitrating the power-performance tradeoff in SaaS clouds," *IEEE Transactions on Parallel and Distributed Systems*, vol. 25, no. 10, pp. 2648–2658, Oct. 2014.

[34] C. L. Gu, Z. L. Li, H. J. Huang, and X. H. Jia, "Energy efficient scheduling of servers with multi-sleep modes for cloud data center," *IEEE Transactions on Cloud Computing*, vol. 8, no. 3, pp. 833–846, Jul./Sep. 2020.

[35] M. Chen, C. W. Gao, M. Song, S. S. Chen, D. Z. Li, and Q. Liu, "Internet data centers participating in demand response: a comprehensive review," *Renewable and Sustainable Energy Reviews*, vol. 117, pp. 109466, Jan. 2020.

[36] H. Wang, J. W. Huang, X. J. Lin, and H. Mohsenian-Rad, "Proactive demand response for data centers: a win-win solution," *IEEE Transactions on Smart Grid*, vol. 7, no. 3, pp. 1584–1596, May 2016.

[37] M. Chen, C. W. Gao, M. Shahidehpour, and Z. Y. Li, "Incentive-compatible demand response for spatially coupled internet data centers in electricity markets," *IEEE Transactions on Smart Grid*, vol. 12, no. 4, pp. 3056–3069, Jul. 2021.

[38] S. R. Chen, P. Li, H. R. Ji, H. Yu, J. Y. Yan, J. Z. Wu, and C. S. Wang, "Operational flexibility of active distribution networks with the potential from data centers," *Applied Energy*, vol. 293, pp. 116935, Jul. 2021.

[39] M. Chen, C. W. Gao, Z. Y. Li, M. Shahidehpour, Q. Zhou, S. S. Chen, and J. L. Yang, "Aggregated model of data network for the provision of demand response in generation and transmission expansion planning," *IEEE Transactions on Smart Grid*, vol. 12, no. 1, pp. 512–523, Jan. 2021.

[40] R. P. Huang, S. J. Qu, Z. W. Gong, M. Goh, and Y. Ji, "Data-driven two-stage distributionally robust optimization with risk aversion," *Applied Soft Computing*, vol. 87, pp. 105978, Feb. 2020.

[41] P. Wang, Y. J. Cao, Z. H. Ding, H. H. Tang, X. Y. Wang, and M. Cheng, "Stochastic programming for cost optimization in geographically distributed internet data centers," *CSEE Journal of Power and Energy Systems*, vol. 8, no. 4, pp. 1215–1232, Jul. 2022.

[42] C. S. Guo, F. J. Luo, Z. X. Cai, and Z. Y. Dong, "Integrated energy systems of data centers and smart grids: state-of-the-art and future opportunities," *Applied Energy*, vol. 301, pp. 117474, Nov. 2021.

[43] R. Snaiki and T. Wu, "Revisiting hurricane track model for wind risk assessment," *Structural Safety*, vol. 87, pp. 102003, Nov. 2020.

[44] P. J. Vickery, F. J. Masters, M. D. Powell, and D. Wadhera, "Hurricane hazard modeling: the past, present, and future," *Journal of Wind Engineering and Industrial Aerodynamics*, vol. 97, no. 7–8, pp. 392–405, Sep./Oct. 2009.

[45] A. G. Davenport, "Rationale for determining design wind velocities," *Journal of the Structural Division*, vol. 86, no. 5, pp. 39–68, May 1960.

[46] C. Uçkun, A. Botterud, and J. R. Birge, "An improved stochastic unit commitment formulation to accommodate wind uncertainty," *IEEE Transactions on Power Systems*, vol. 31, no. 4, pp. 2507–2517, Jul. 2016.

[47] P. F. Zhao, C. H. Gu, D. Huo, Y. C. Shen, and I. Hernando-Gil, "Two-stage distributionally robust optimization for energy hub systems," *IEEE Transactions on Industrial Informatics*, vol. 16, no. 5, pp. 3460–3469, May 2020.

[48] A. Gandhi, M. Harchol-Balter, and M. A. Kozuch, "The case for sleep states in servers," in *Proceedings of the 4th Workshop on Power-Aware Computing and Systems*, 2011, pp. 2.

[49] S. W. Liu, T. Y. Zhao, X. Liu, Y. Z. Li, and P. Wang, "Proactive resilient day-ahead unit commitment with cloud computing data centers," *IEEE Transactions on Industry Applications*, vol. 58, no. 2, pp. 1675–1684, Mar./Apr. 2022.

[50] Z. Chen, L. Wu, and Z. Y. Li, "Electric demand response management for distributed large-scale internet data centers," *IEEE transactions on Smart Grid*, vol. 5, no. 2, pp. 651–661, Mar. 2014.

[51] Y. X. Guo, Y. M. Gong, Y. G. Fang, P. P. Khargonekar, and X. J. Geng, "Energy and network aware workload management for sustainable data centers with thermal storage," *IEEE Transactions on Parallel and Distributed Systems*, vol. 25, no. 8, pp. 2030–2042, Aug. 2014.

[52] P. M. Subcommittee, "IEEE reliability test system," *IEEE Transactions on Power Apparatus and Systems*, vol. PAS-98, no. 6, pp. 2047–2054, Nov. 1979.

[53] H. J. Zhang, L. Cheng, S. H. Yao, T. Y. Zhao, and P. Wang, "Spatial–temporal reliability and damage assessment of transmission networks under hurricanes," *IEEE Transactions on Smart Grid*, vol. 11, no. 2, pp. 1044–1054, Mar. 2020.

[54] Logs of real parallel workloads from production systems. [Online]. Available: https://www.cse.huji.ac.il/labs/parallel/workload/lkitfh2/index.html

[55] (2022). Atlantic hurricane database (HURDAT2) 1851–2021. [Online]. Available: https://www.nhc.noaa.gov/data/#hurdat

[56] S. Y. Tao, Q. S. Xu, A. Feijóo, and G. Zheng, "Joint optimization of wind turbine micrositing and cabling in an offshore wind farm," *IEEE Transactions on Smart Grid*, vol. 12, no. 1, pp. 834–844, Jan. 2021.

[57] R. E. Gomory, "An algorithm for the mixed integer problem," The Rand Corporation, Tech. Report RM-2597, 1960.

[58] H. Marchand and L. A. Wolsey, "Aggregation and mixed integer rounding to solve mips," *Operations Research*, vol. 49, no. 3, pp. 363–371, Jun. 2001.

[59] Z. h. Gu, G. L. Nemhauser, and M. W. P. Savelsbergh, "Lifted flow cover inequalities for mixed 0–1 integer programs," *Mathematical Programming*, vol. 85, no. 3, pp. 439–467, Aug. 1999.

[60] J. F. Bender, "Partitioning procedures for solving mixed-variables programming problems," *Numerische Mathematik*, vol. 4, no. pp. 238–252, Dec. 1962.

Shengwei Liu received the B.Eng. and M.Eng. degrees in Electrical Engineering from Guangdong University of Technology, Guangzhou, China, in 2017 and 2020, respectively. He is currently working toward the Ph.D. degree in Electrical Engineering at the Energy and Electricity Research Center, Jinan University, Zhuhai, China. His research interests include smart grid resilience and operation research.

Tianyang Zhao received the B.Eng., M.Eng., and Ph.D. degrees in Electrical Engineering from North China Electric Power University, Beijing, China, in 2011, 2013, and 2017, respectively. He was a Postdoctoral Research Fellow with the Energy Research Institute, Nanyang Technological University, Singapore, from 2017 to 2020. His research interests include operation research and resilience.

Xuan Liu received the B.Sc. degree from University of San Francisco in 2015 and the M.Sc. degree in Electrical Engineering from Washington State University in 2019. Currently he is pursuing his Ph.D. degree in Electrical Engineering at the Electricity and Energy Research Institute, Jinan University, Zhuhai, Guangzhou, China. His research interests include deep learning, optimization, and explainable AI.

Yuanzheng Li received the M.S. degree from the Huazhong University of Science and Technology (HUST) in 2011, Wuhan, China, and the Ph.D. degree from the South China University of Technology (SCUT), Guangzhou, China, in 2015, both in Electrical Engineering. He is currently an Associate Professor with HUST. He has authored or coauthored several peer-reviewed papers in international journals. His current research interests include artificial intelligence and its application in smart grid, optimal power system dispatch and decision making, stochastic optimization considering large-scale integration of renewable energy into the power system, and multiobjective optimization.

Peng Wang received the B.Sc. degree in Electronic Engineering from Xi'an Jiaotong University, Xi'an, China, in 1978, the M.Sc. degree from the Taiyuan University of Technology, Taiyuan, China, in 1987, and the M.Sc. and Ph.D. degrees in Electrical Engineering from the University of Saskatchewan, Saskatoon, SK, Canada, in 1995 and 1998, respectively. He is currently a Professor with the School of Electrical and Electronic Engineering, Nanyang Technological University, Singapore.